Characterization of Magnetic Steels for the FCC-ee Magnet Prototypes

Characterization of Magnetic Steels for the FCC-ee Magnet Prototypes

Jaime R. Anglada
Technology Department
Magnets, Superconductors and Cryostats Group
CERN
Geneva, Switzerland
jaime.renedo@cern.ch

Pasquale Arpaia
Department of Electrical Engineering and Information Technology
University of Naples Federico II
Naples, Italy
pasquale.arpaia@unina.it

Marco Buzio
Technology Department
Magnets, Superconductors and Cryostats Group
CERN
Geneva, Switzerland
marco.buzio@cern.ch

Mariano Pentella
Department of Applied Science and Technology
Polytechnic of Turin
Turin, Italy
mariano.pentella@polito.it

Carlo Petrone
Technology Department
Magnets, Superconductors and Cryostats Group
CERN
Geneva, Switzerland
carlo.petrone@cern.ch

***Abstract*—At the European Organization for the Nuclear Research (CERN), several efforts were combined for a preliminary design of a new accelerator, the Future Circular Collider (FCC), a 100-TeV double-ring hadron collider to be installed in a 100-km tunnel. As potential intermediate step, a high-luminosity lepton collider called FCC-ee is foreseen with more than 9,000 magnets. This paper provides an insight into the magnetic properties of the steels, potentially considered for the new dipole magnets, with nominal field of only 56 mT. The influence of the properties of these steels on the magnet transfer function has been assessed analytically using an equivalent reluctance network to model the first 1-m long dipole prototypes. The analytical results were validated experimentally. The proposed approach can be a useful tool for traceability and quality control during the series production.**

***Index Terms*—split-coil permeameter, coercive field, magnetic measurements, Future Circular Collider**

I. Introduction

The Large Hadron Collider (LHC) [1] currently in operation at the European Organization for the Nuclear Research (CERN) and its future high-luminosity upgrade, the HL-LHC [2] have a program that extends over the next 15 years. Considering that the design, construction and commissioning of a large machine such as the LHC required 30 years, the necessity of preparing the next accelerator for the post-LHC era was particularly urgent. For this reason, according to the European strategy for Particle Physics 2013 [3], the efforts were combined into the Future Circular Collider study, carried out by CERN. The long-term goal of the Future Circular Collider is the construction of a 100 TeV double-ring hadron collider (FCC-hh) to be installed in a 100-km long tunnel [4]. As a potential intermediate step, a high-luminosity lepton collider (FCC-ee) was considered [5], as it had already been done in the past with the construction of the Large Electron-Positron collider (LEP) prior the LHC [6].

FCC-ee is a double-ring synchrotron, colliding electrons and positrons at energies in the range from 40 up to 175 GeV [7]. According to the preliminary design of the beam optics [8], the magnets necessary to bend and focus the beam, it includes more than 6000 60-mT dipole magnets and about 3000 quadrupole magnets with 8.8 T/m nominal field gradient for the focusing quadrupoles and 21.8 T/m for the defocusing quadrupoles. The nominal field of the focusing quadrupole is lower because they are longer, in order to reduce the radiation emitted in the horizontal plane. Given the low fields, the choice has been the adoption of resistive magnets.

As reported in [9], LEP had 108 mT C-shaped dipole magnets with steel-concrete cores, with a percentage of steel of only 27% in order to optimize the operational point of the steel with respect to the peak permeability and mainly to reduce the costs. The quadrupole magnets, having a gradient of roughly 10 T/m, were made of classical iron core. Another alternative, such as it was considered in the Extra Low ENergy Antiproton ring (ELENA), could be the yoke dilution with stainless steel but field quality and remanent field degrades [10], [11]. In HERA (Hadron-Electron Ring Accelerator), hosted at the Deutsches Elektronen-Synchrotron (DESY) [12] they employed C-shaped magnets with the yoke made of 5 mm thick punched laminations.

According to these considerations, Milanese in [13] proposed a first concept design of the FCC-ee dipole and quadrupole magnets. For the production of the first magnet prototypes, two steels have been considered: a high-quality low-carbon steel such as ARMCO®, already employed for the upgrade of the LHC superconducting dipole and quadrupole magnets

[14], [15] and S355 J2+N, a low-cost structural steel. The goal of this paper is to present the characterization of the magnetic properties of these two steels. The overall effect on the dipole magnet was then assessed and the results compared with the results obtained in a previous magnetic measurement campaign.

II. Measurement method

In the following, (i) the *sample preparation and measurement system*, (ii) the *initial magnetization curve*, and (iii) the *coercive field and residual flux density curve* are presented.

A. Sample preparation and measurement system

The reference standard for the DC characterization of soft magnetic material is the standard IEC 60404-4 [16]. The layout of the measurement system is shown in Fig. 1. The

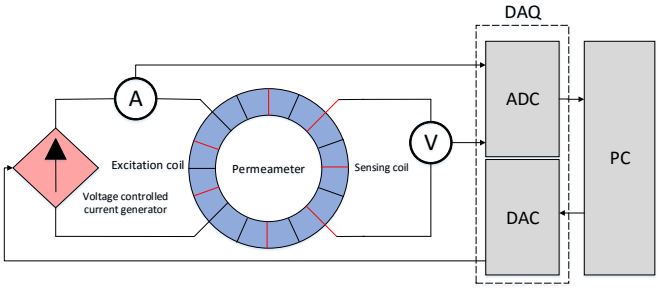

Fig. 1. Architecture of the measurement system [15].

measurement method is based on the CERN split-coil permeameter. This method allows to measure the magnetic properties of soft magnetic materials without the time-demanding operation of winding the specimen [17]. The test specimen is magnetized by two excitation coils, made of 90 turns and powered in series by a voltage-controlled current generator. A 90-turns sensing coil detects the induced voltage. The whole apparatus is cooled by compressed air.

Although the measurement of the initial magnetization curve is compliant with the standard [16], the coercive field and residual flux density are determined differently because the sample is prepared according to the CERN internal procedure [18]. In fact, given d_2 and d_1 respectively inner and outer diameter of the specimen, the standard prescribes $d_2/d_1 \leq 1.1$ to neglect the effect of the eddy currents. This shrinks the hysteresis loop and reduces the uncertainty estimation of the coercive field and residual flux density.

The test specimens are prepared with a ratio $d_2/d_1 = 1.5$, with 114 mm outer diameter, 76 mm inner diameter and thickness 15 mm. All of the specimens are cut by the main sheet coil by water jet method in order to not alter the magnetic properties of the steel.

B. Initial magnetization curve

The initial magnetization curve is measured by using the fluxmetric method and in particular by adopting the *point-by-point* method proposed by the standard IEC 60404-4 [16]. The *point-by-point* method consists in powering the excitation coils by ramping the current back and forth between positive and negative symmetric values. Each ramp is followed by a plateau where the current is kept constant for the time necessary to extinguish the transient due to the eddy currents. The amplitude of the plateau is then increased at each cycle, as shown in Fig. 2a. During the excitation, the current in the excitation coil and the induced voltage in the sensing coil are continuously recorded. The sample is demagnetized between each magnetization cycle and the next.

The reference voltage used to control the power supply is generated by means of a digital-to-analog converter embedded in the acquisition system (DAQ). The DAQ communicates with a PC, where a suite of interactive programs developed in $C++$ (Flexible Framework for Magnetic Measurements [19]) manages the whole measurement process.

The magnetic field $H(t)$ generated from the current $i(t)$ carried by the excitation coil is

$$H(t) = \frac{N_e i(t)}{2\pi r_0} \tag{1}$$

where N_e is the total number of turns of the excitation coils and r_0 is the log-mean radius of the specimen. The magnetic field is considered uniform in the cross-sectional area of the specimen.

The magnetic flux density, B, is estimated by integrating the induced voltage v_s on the sensing coil. Neglecting the initial magnetic state of the specimen, thus assuming a perfect demagnetization

$$\Phi = \int_{t_0}^{t} v_s(\tau) d\tau \tag{2}$$

where Φ is the linked flux with N_t turns of the sensing coil. This yields to the expression of the magnetic flux density B

$$B(t) = \frac{1}{A_s}\left(\frac{\Phi(t)}{N_t} - \mu_0 H(t) A_a\right) \tag{3}$$

where A_s is the cross-sectional area of the specimen. Given A_t the cross-sectional area of the coil, $A_a = A_t - A_s$ is the portion of area occupied by the air.

The (H_i, B_i) points of the initial magnetization curve are evaluated in correspondence of the tip points of the nested hysteresis loops, as shown in Fig. 2b. The tip points correspond to the excitation current plateaux and the evaluation is performed in correspondence of the zero points of the voltage, after the damping of the eddy currents.

From these points, the relative permeability is calculated as:

$$\mu_{r_i} = \frac{B_i}{\mu_0 H_i} \tag{4}$$

C. Coercive field and residual flux density curve

The coercive field and the residual flux density were evaluated by applying different symmetrical excitation cycles, with increasing amplitude but keeping the current ramp rate constant. The measurement was done at four ramp rates:

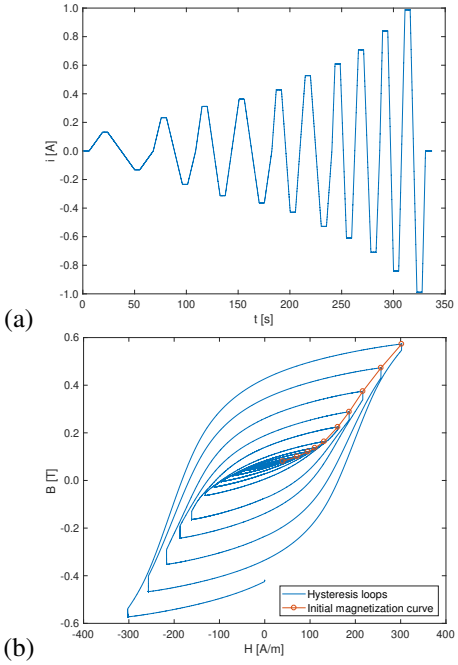

Fig. 2. Test excitation current used for the test (a), and hysteresis loops (b): in red, the evaluated initial magnetization curve, measured on the S355 sample.

1025, 1554, 3067 and 6135 A/(m s). The lowest value was chosen for thermal and measurement time reasons. The highest value corresponds to the maximum current ramp rate of the power supply. The coercive field in DC was finally evaluated by extrapolation from the experimental data, fitted with a polynominal law from [20]:

$$H_{ck}(R) = H_{ck}(0) + b_k\sqrt{R} + c_k R \tag{5}$$

$$B_{rk}(R) = B_{rk}(0) + b_k\sqrt{R} + c_k R \tag{6}$$

where R is the ramp rate, $H_c(0)$ is the DC coercive field, $Br(0)$ the DC residual flux density, b, c, d and e the coefficients of the polynomial used for the fitting. The terms $b_k\sqrt{R}$ and $c_k R$ describe the normal and the anomalous eddy currents. Each point $H_{ck}(R)$ and $B_{rk}(R)$ was measured in correspondence of the zero points of the magnetic flux density and of the magnetic field respectively.

III. Experimental Results

A. Characterization of ARMCO® and S355

All the samples were tested at room temperature. Fig. 3 and Fig. 4 shows the results of the measurements performed on the ARMCO® sample.

The material properties are consistent with the expectations for a non-annealed low-carbon steel such as ARMCO®, containing less than the 0.01% of carbon content, with a peak relative permeability of 3621, a saturation point of 1.6835 T at 3379.30 A/m. The hysteresis loop parameters are a coercive field of 200.53 A/m and a residual flux density of 0.9480 T on the major loop.

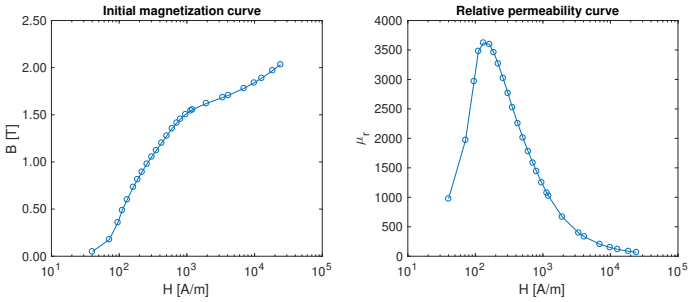

Fig. 3. Initial magnetization curve (left) and relative permeability curve (right) of ARMCO®.

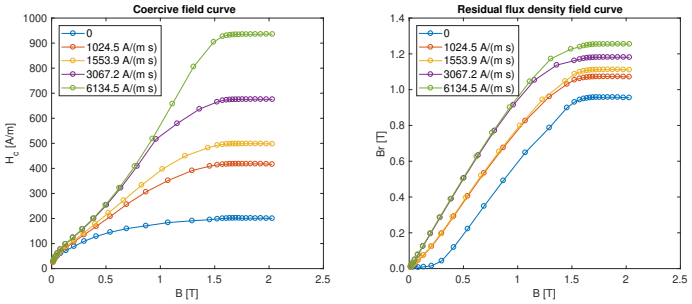

Fig. 4. Coercive field curves (left) and residual flux density curves (right) for the ARMCO® sample as a function of the initial magnetic flux density in the material cross-section, measured at different ramp rates (values at $R = 0$ retrieved by extrapolation).

Fig. 5-7 show the results of the measurements performed on the two S355 sample.

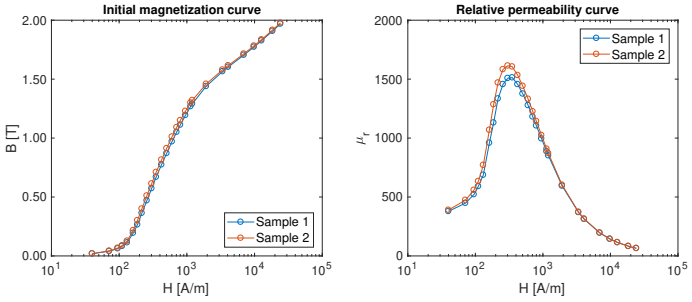

Fig. 5. Initial magnetization curve (left) and relative permeability curve (right) of the two samples of S355.

The S355 steel, due to its higher carbon content (0.17%), presents worse magnetic properties than the ARMCO® sample. The two samples properties are:

- Sample 1 has a relative peak permeability of 1614, a saturation point of 1.7046 T at 6946.50 A/m. The hysteresis loop parameters are a coercive field of 315.33 A/m and a residual flux density of 0.9694 T on the major loop
- Sample 2 has a relative peak permeability of 1513, a saturation point of 1.7149 T at 6945.80 A/m. The hysteresis loop parameters are a coercive field of 309.80 A/m and a residual flux density of 1.0057 T on the major loop.

The magnetic properties of the two S355 samples are similar

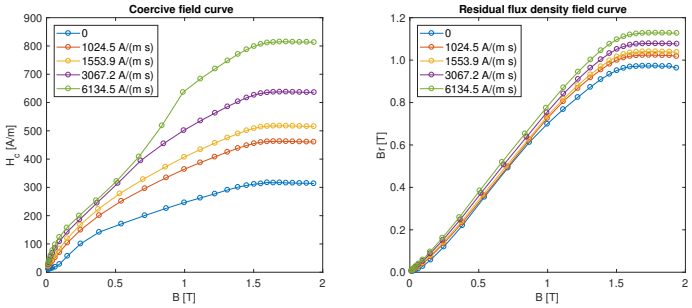

Fig. 6. Coercive field curves (left) and residual flux density curves (right), for the S355 sample (sample 1) as a function of the initial magnetic flux density in the material cross-section, measured at different ramp rates (values at $R = 0$ retrieved by extrapolation).

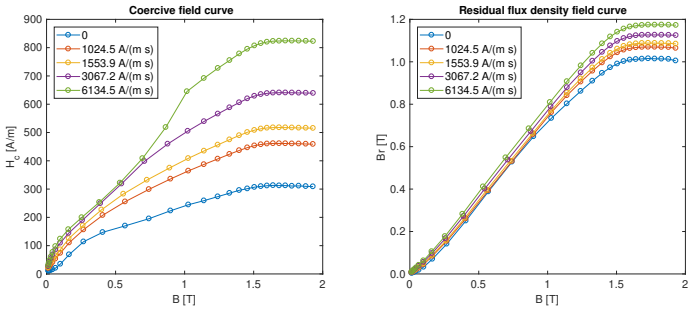

Fig. 7. Coercive field curves (left) and residual flux density curves (right), for the S355 sample (sample 2) as function of the initial magnetic flux density in the material cross-section, measured at different ramp rates (values at $R = 0$ retrieved by extrapolation).

with the permeability peaks that differ of roughly the 5%. By comparing the magnetic properties of the structural steel with the one of the ARMCO®, the latter behaves magnetically better, having more than twice the peak permeability and a lower coercivity value. Hence, the quadrupole magnet prototype has the yoke made of ARMCO®, in order to guarantee the value of the nominal field gradient and the necessary field quality. For the dipole magnets, considered the extremely low operation field, S355 is an interesting option since it costs about five times less, has a coercive field of only about 60% higher than ARMCO® and similar residual flux density.

B. Effects on the dipole magnet prototypes

A study on the effects of the materials properties on the first 1-m long dipole prototypes was carried out. Two identical prototypes were respectively made of ARMCO® and S355. The magnets are twin aperture with air-gap length of 84 mm, I-shaped and made of two plates connected by 9 cylinders in the center. The magnet excitation current is carried by a single central copper bus bar. A picture of one of the magnets is shown in Fig. 8.

The study was carried out by considering an equivalent reluctance network, shown in Fig. 9. The results of the model were finally compared with the magnetic measurements, performed by rotating coil method, whose results are reported in [21].

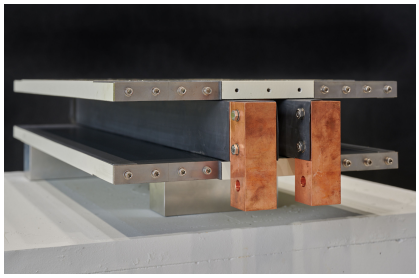

Fig. 8. The 1-m dipole magnet prototype.

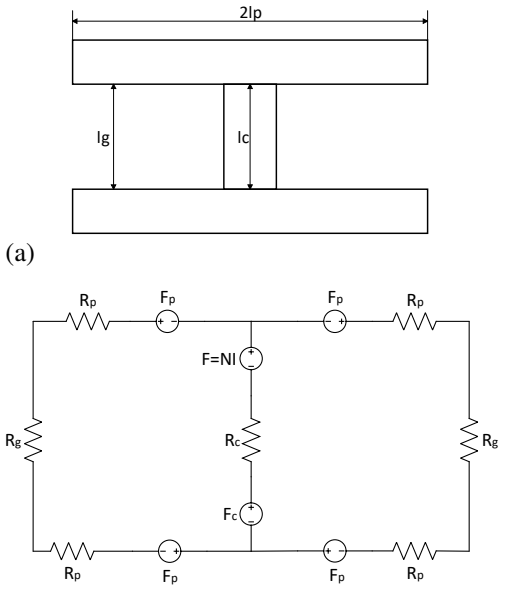

Fig. 9. Magnet mechanical design (a) and reluctance network model (b).

$F = NI$ is the excitation magnetomotive force generated by the magnet coil. The 9 cylinders were represented with their equivalent parallel circuit with $F_c = H_{cc} l_c$ the magnetomotive force due to the coercive field level in the cyclindrical branches H_{cc}. l_c is the length of the cylindrical branches and R_c their equivalent reluctance. $F_p = H_p l_p$ is the magnetomotive force due to the coercive field level in the magnet plates H_{cp}. l_p is the half-plate length and R_p is the half-plate reluctance. R_g is the air-gap reluctance.

All the parameters were assigned from the material measurements iteratively. Assigned the current, the flux density value in each branch was evaluated. This was then used to retrieve the values of relative permeability in order to evaluate the reluctances and the values of coercive field and calculate F_p and F_c. The flux densities were then evaluated again and compared with the previous value. The procedure was repeated until the reaching of the assigned convergence criteria. Finally, the model output is the magnetic flux density across the air-gap reluctances.

The results are summarized in Tables I-II. Only three operation conditions were considered: without current, at the minimum

operation current $I = 1000$ A, at $I = 2500$ A and close to the nominal current $I = 3500$ A. All the points were evaluated twice: by taking into account a magnet pre-cycling after the demagnetization, consisting of five current cycles from $NI = 4500$ A to $NI =$ -4500 A and without pre-cycling. The considered coercive field values when studying the pre-cycling are the one evaluated by assigning $NI = 4500$ A. In absence of pre-cycling, the coercive field values are the one corresponding to the previous applied NI. For the magnet made of S355, the magnetic properties of the sample 1 were considered.

TABLE I
COMPARISON BETWEEN SIMULATED AND MEASURED FIELD ON THE PROTOTYPE MADE OF ARMCO®

MMF NI [A]	Pre-cycling	B [mT]	Measured B [mT]
0	NO	0.066	0.068
	YES	0.980	0.575
1000	NO	13.94	13.51
	YES	13.41	13.50
2500	NO	35.65	34.36
	YES	35.43	34.38
3500	NO	49.95	47.77
	YES	49.95	47.78

TABLE II
COMPARISON BETWEEN SIMULATED AND MEASURED FIELD ON THE PROTOTYPE MADE OF S355

MMF NI [A]	Pre-cycling	B [mT]	Measured B [mT]
0	NO	0.011	0.014
	YES	1.262	1.467
1000	NO	13.00	12.76
	YES	12.22	12.55
2500	NO	34.26	33.24
	YES	34.10	33.27
3500	NO	48.46	46.20
	YES	48.36	46.26

Both models show consistent results with the magnetic measurements, showing an overall difference between measured and simulated field between 2 and 4%. This because considering the low field values delivered by the magnets, the highest contribution in the aperture is provided by the coil. Nevertheless, observing the values of the residual field, there is an important difference between the measured and the simulated value for the prototype made of ARMCO®, where the difference is of about the 180% whereas for the S355 the difference is only of 16%. A possible explanation is that the Pure Iron used to build the magnet may be different from the measured one, considering also that this material is highly sensitive to the environmental conditions such as mechanical and thermal stress. Hence, it is likely that the ARMCO® used to produce the sample and the one used to build the magnet prototype were not from the same coil of material.
In [21], the yoke coercive fields were evaluated by the following formula, also used in [22] about the LEP magnets production :

$$H_c = \frac{(\Delta TF)hNI}{\mu_0 l_{iron}} \tag{7}$$

where ΔTF is the difference between the values of the transfer functions at the beginning and at the end of the current ramping cycle, h is the air-gap length, l_{iron} the magnetic path length. The values of the coercive field on the major loop were of 150 A/m for the ARMCO® and 340 A/m for the S355. Hence, the results are consistent with the S355 sample.
The values of the residual field when the magnets are not pre-cycled are consistent with the measured ones because the coercive field values after the degaussing are the minimum ones and with roughly the same value (15 A/m for the ARMCO® against 17 A/m for the S355).

IV. CONCLUSIONS

The characterization of two magnetic steels, respectively a low-carbon steel such as ARMCO® and structural low-cost steel such as S355, for the manufacturing of the FCC-ee magnet prototypes, is presented. The magnetic measurement campaign, carried out at CERN, showed that the two considered steels exhibit comparable behavior, though ARMCO® presents a higher relative peak permeability and lower coercive field value due to its lower carbon content. This lead to the conclusion that S355 can be considered as low-cost solution to produce the FCC-ee dipole magnets whereas ARMCO® can be considered for the production of the quadrupole magnets.
Finally, the results of the magnetic characterization were used to check the effects on the 1-m long dipole magnet and the simulation results compared with the magnetic measurements performed in [21]. The comparison showed an inconsistency on the prototype made of ARMCO® due to the different values of coercive field between the measured one and the one used to build the magnet. The hypothesis is that the material specimen and the yoke material were likely from two different lots of material, considering also the high sensitivity of the iron to factors such as mechanical or thermal stress, that can modify the magnetic properties. Hence, a further investigation is required in order to check the production process. On the other hand, the results obtained for the prototype made of S355 are consistent, showing that this material is more stable. The conclusion is that this cross-checking method may be used in the future to perform quality control during the series production of the magnets because their reproducibility depends mainly on the yoke material and occurring modifications of its magnetic properties can be easily detected.

REFERENCES

[1] L. Evans, "The Large Hadron Collider," *New Journal of Physics*, vol. 9, no. 9, p. 335, 2007.
[2] L. Rossi, O. Brüning *et al.*, "High luminosity Large Hadron Collider," in *European Strategy Preparatory Group-Open Symposium, Krakow*, 2012.
[3] M. Krammer, "The update of the European strategy for particle physics," *Physica Scripta*, vol. 2013, no. T158, pp. 014 019–1–7, 2013.
[4] M. Benedikt and F. Zimmermann, "Status and challenges of the future circular collider study," Tech. Rep., 2016.
[5] A. Abada, T. Sjöstrand, and P. Skands, "Future circular collider: Vol. 2 the lepton collider (fcc-ee)," 2019.

[6] S. Myers and E. Picasso, "The design, construction and commissioning of the CERN Large Electron–Positron collider," *Contemporary Physics*, vol. 31, no. 6, pp. 387–403, 1990.

[7] J. Wenninger *et al.*, "Specification: Future circular collider study–lepton collider parameters."

[8] K. Oide, M. Aiba, S. Aumon, M. Benedikt, A. Blondel, A. Bogomyagkov, M. Boscolo, H. Burkhardt, Y. Cai, A. Doblhammer *et al.*, "Design of beam optics for the future circular collider e+ e- collider rings," *Physical Review Accelerators and Beams*, vol. 19, no. 11, p. 111005, 2016.

[9] L. Resegotti, "The lep magnet system," *Le Journal de Physique Colloques*, vol. 45, no. C1, pp. C1–233, 1984.

[10] D. Schoerling, "Case study of a magnetic system for low-energy machines," *Physical Review Accelerators and Beams*, vol. 19, no. 8, p. 082401, 2016.

[11] C. Carli, L. Fiscarelli, and D. Schoerling, "Considerations on the effect of magnet yoke dilution on remanent field at ELENA," 2017.

[12] G. Voss and B. Wiik, "The electron-proton collider hera," *Annual Review of Nuclear and Particle Science*, vol. 44, no. 1, pp. 413–452, 1994.

[13] A. Milanese, "Efficient twin aperture magnets for the future circular e+/e- collider," *Physical Review Accelerators and Beams*, vol. 19, no. 11, p. 112401, 2016.

[14] A. Parrella, P. Arpaia, M. Buzio, A. Liccardo, M. Pentella, R. Principe, and P. Ramos, "Magnetic properties of pure iron for the upgrade of the lhc superconducting dipole and quadrupole magnets," *IEEE Transactions on Magnetics*, vol. 55, no. 2, pp. 1–4, 2018.

[15] P. Arpaia, M. Buzio, S. I. Bermudez, A. Liccardo, A. Parrella, M. Pentella, P. M. Ramos, and E. Stubberud, "A superconducting permeameter for characterizing soft magnetic materials at high fields," *IEEE Transactions on Instrumentation and Measurement*, 2019.

[16] IEC, *Magnetic materials-Part 4: Methods of measurement of dc magnetic properties of magnetically soft materials*, IEC 60404-4, IEC Std.

[17] P. Arpaia, M. Buzio, L. Fiscarelli, G. Montenero, and L. Walckiers, "High-performance permeability measurements: A case study at cern," in *2010 IEEE Instrumentation & Measurement Technology Conference Proceedings*. IEEE, 2010, pp. 58–61.

[18] M. Pentella, "Test procedure for the DC magnetic characterization of ring-samples of soft magnetic materials," CERN, Geneva, Internal Note EDMS 2215570, 2019.

[19] P. Arpaia, M. Buzio, L. Fiscarelli, and V. Inglese, "A software framework for developing measurement applications under variable requirements," *Review of Scientific Instruments*, vol. 83, no. 11, p. 115103, 2012.

[20] R. Grossinger, N. Mehboob, D. Suess, R. S. Turtelli, and M. Kriegisch, "An eddy-current model describing the frequency dependence of the coercivity of polycrystalline galfenol," *IEEE Transactions on Magnetics*, vol. 48, no. 11, pp. 3076–3079, 2012.

[21] A. Milanese, J. Bauche, and C. Petrone, "Magnetic measurements campaign of the first short models of twin aperture magnets for FCC-ee," *Submitted*, 2019.

[22] J. Gourber and L. Resegotti, "Implications of the low field levels in the lep magnets," *IEEE Transactions on Nuclear Science*, vol. 26, no. 3, pp. 3185–3187, 1979.